Quaternary Science Advances 11 (2023) 100095

Contents lists available at ScienceDirect

Quaternary Science Advances

journal homepage: www.sciencedirect.com/journal/quaternary-science-advances

Remote sensing and GIS-based landslide susceptibility mapping using LNRF method in part of Western Ghats of India

Abhijit S. Patil [a,*], Sachin S. Panhalkar [a,b]

[a] Department of Geography, Shivaji University, Kolhapur, India
[b] Center for Climate Change and Sustainability Studies, Shivaji University Kolhapur, India

ARTICLE INFO

Keywords:
LNRF
GIS
Landslide
Western ghats

ABSTRACT

Every year, the Western Ghats region experiences devastating landslides, resulting in significant loss of life and damage to both private and public assets. To mitigate these losses, it is essential to identify the areas most susceptible to landslides. This research aims to create an accurate landslide susceptibility map for a section of the Western Ghats region by employing a comprehensive approach that combines remote sensing and geographical information systems (GIS). The Landslide Numerical Risk Factor (LNRF) method is utilized to determine landslide susceptibility zones. The LNRF model incorporates a landslide inventory based on geographic object-based image analysis and influencing factors. The resulting LNRF model generates a landslide susceptibility map, classifying over 35% of the study region's land area as having a high probability of landslides. The model's accuracy is assessed using the receiver operating characteristic (ROC) method, which yields an area under the curve (AUC) value of 0.77. This indicates that the LNRF model exhibits good predictive performance, resulting in a reliable landslide susceptibility map.

1. Introduction

Landslides are sudden and highly detrimental natural hazards that pose significant threats to human life, infrastructure, economic development, and property. They are considered one of the most frequent and severe natural disasters, causing widespread damage and endangering individuals and communities (Guzzetti et al., 1999; Hadji et al., 2017; Patil et al., 2020). According to the World Health Organization (WHO), landslides account for approximately 12% of all natural disasters, resulting in over 11,500 fatalities and $4.5 billion worth of economic losses annually (Froude and Petley, 2018; WHO, 2022). India, with its unique geographic and geological conditions such as unstable soil and rock formations, intense rainfall, and seismic activities, is particularly prone to landslides (Raj and Chandrasekar, 2016; Bhandari et al., 2020). The Western Ghats region, situated along India's west coast, is one of the most landslide-vulnerable areas in the country, experiencing a high incidence of landslides each year (Raj and Chandrasekar, 2016; Bhandari et al., 2020).

The undulating and mountainous terrain of the Himalayas and Western Ghats in India are well-known features of the country's landscape. Numerous studies on landslide mapping have identified these areas as highly susceptible to landslides and designated them as high-risk zones for such natural disasters (Ramachandra et al., 2010; Srivastava et al., 2010; Patil and Panhalkar, 2019; Patil et al., 2020; Patil et al., 2022). Additionally, climate change has emerged as a significant factor affecting landslide occurrences worldwide (Iverson, 2018). Climate change-induced factors, such as intense rainfall, increased temperature, and sea-level rise, have a substantial impact on landslide susceptibility and frequency (Sidle et al., 2018). Therefore, it is essential to consider the effects of climate change while developing Landslide Susceptibility Mapping (LSM) models to ensure accurate and reliable predictions.

Landslide susceptibility refers to the probability of landslides occurring in different geographic locations (van Westen et al., 2006; Guzzetti et al., 2006). By utilizing various landslide prediction models, it may be possible to mitigate damages caused by landslides to some extent (Pradhan and Lee, 2010). In the past two decades, significant developments in processing power, remote sensing (RS), and geographic information systems (GIS) have made it easier to prepare landslide susceptibility maps (Achour and Pourghasemi, 2020). These advances have revolutionized the field of landslide studies (Lee, 2019; Shano et al., 2020; Patil et al., 2020; Pradhan et al., 2020, 2021; Coco et al., 2021; Hodasova and Bednarik, 2021).

* Corresponding author.
E-mail addresses: abhijitpatil8893@gmail.com (A.S. Patil), panhalkarsachin@gmail.com (S.S. Panhalkar).

https://doi.org/10.1016/j.qsa.2023.100095
Received 6 March 2023; Received in revised form 16 June 2023; Accepted 19 June 2023
Available online 26 June 2023
2666-0334/© 2023 The Authors. Published by Elsevier Ltd. This is an open access article under the CC BY license (http://creativecommons.org/licenses/by/4.0/).

The urgency for accurate landslide susceptibility mapping in the Western Ghats region was emphasized by the devastating landslides in Taliye village in 2021, resulting in the loss of over 84 lives (Vallabh, 2021; Inamdar, 2021). Such mapping is crucial for minimizing infrastructure damage and loss of human life. Therefore, several researchers have employed landslide susceptibility mapping as a vital first step in the strategy, evaluation, and mitigation of landslides. Numerous studies, including Dai et al. (2001), Lee (2005), Pradhan et al. (2010), Constantin et al. (2011), and Patil et al. (2022), have utilized this method to produce landslide vulnerability maps. However, the landslide vulnerability maps created in India thus far have primarily focused on key transportation routes and specific locations in highly susceptible states. Hence, it is essential to develop and map landslide susceptibility at different spatial scales to effectively manage landslide risks (Persichillo et al., 2016). Such mapping can aid in risk mitigation strategic planning, the implementation of monitoring and early warning systems, and the formulation of sustainable and efficient land-use plans for authorities and planners (Roccati et al., 2021).

In recent years, various RS and GIS-based models have been employed to estimate landslide vulnerability. Among these models, both qualitative and quantitative approaches have been widely used (Devkota et al., 2013; Wang et al., 2016). One such quantitative method is the Landslide Numerical Risk Factor (LNRF) model, which offers a convenient and highly accurate way to map susceptibility classes for landslides across different influencing factors. The LNRF method has been extensively utilized by researchers globally to investigate the relationship between previous landslide events and various subclasses of potentially influential factors. According to Ali Mohammadi et al. (2014), the LNRF model is particularly suitable for analyzing landslide susceptibility in mountainous regions. Thus, the objective of this study is to employ the LNRF model to produce a landslide susceptibility map in the Western Ghats, a mountainous terrain located in India.

2. Study region

The study region is located in the southernmost portion of Maharashtra, encompassing the basins of the Bhogawati (Phonda Ghat) river and Ghataprabha river (Amboli Ghat). It includes two districts, namely Kolhapur (Radhanagari, Bhudargad, Ajara, and Chandgad Tehsils) and Sindhudurg (Kankauli, Kudal, and Savantvadi Tehsils). Geographically,

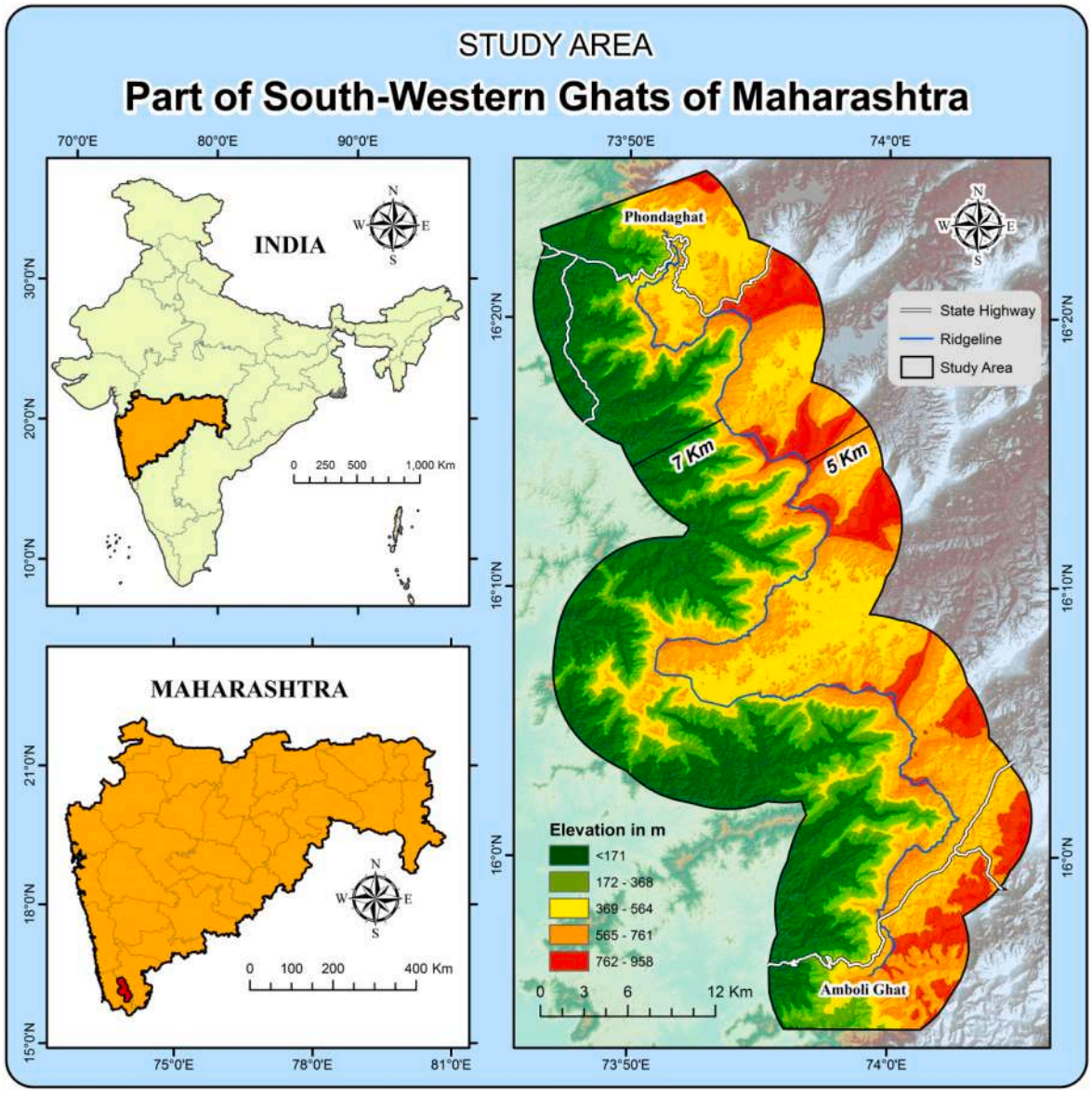

Fig. 1. Geographical Location of Study region.

the study region spans from 15° 53′ to 16° 25′ North latitude and 73° 45′ to 75° 05′ East longitude, covering an area of approximately 1083 km^2, which represents 0.35% of the total area of Maharashtra state (Fig. 1). The study region experiences an average yearly precipitation of around 4200 mm. It exhibits variations in elevation, with the western part characterized by lower elevations and the eastern part featuring higher elevations.

3. Material and methods

Landslide susceptibility zonation mapping in the study region involves the following steps: a) Identification of past landslide events; b) Mapping of the layers of factors that influence landslides; c) Use of the LNRF model to map the susceptibility of landslides; and d) Evaluation of the accuracy of the susceptibility mapping. The research flowchart implemented in the present study is depicted in Fig. 2.

3.1. Landslide inventory map

An inventory map of landslides provides valuable information on the spatial patterns of landslide incidents within a given area, enhancing our understanding of the correlation between the distribution of landslides and the influencing factors associated with them (Abdo, 2022; Hong et al., 2015). Mapping the historical and current locations of landslides is a crucial initial step in creating susceptibility maps for an area (Hungr et al., 2005). Recent evidence from satellite images, on-site observations, and research (Ajin et al., 2022; Vasudevan et al., 2022; Sarun et al., 2021) indicates a significant increase in the number of landslide incidents in the Western Ghats region in recent years.

For this research project, the mapping of landslides is conducted using the geographic object-based image analysis (GEOBIA) approach. GEOBIA enhances the accuracy of landslide inventory mapping and detection of changes from multi-temporal satellite images (Blaschke et al., 2014). By analyzing pre- and post-event very high-resolution satellite images, spectral and/or morphological variations can be observed, enabling the detection of new or rejuvenated landslides (Daniel et al., 2015; Patil et al., 2020). Martha et al. (2012) proposed a semi-automated OBIA method for creating historical landslide inventories based on brightness changes in pre- and post-event satellite images. The increase in brightness in landslide regions resulting from the exposure of fresh soil and rocks on the earth's surface can be detected by comparing pre- and post-event satellite images using the GEOBIA-based automated technique. This approach is used to map the landslide inventory from 2014 to 2019. Influencing factors are prepared for landslide susceptibility modeling, and LNRF simulation is performed using a combination of the landslide inventory and influencing factors.

The GEOBIA method is employed to extract landslides for inventory mapping. Using a semi-automated approach, 58 landslides are detected from 2014 to 2019, and the results are presented as a landslide inventory map of the southwestern Ghats of Maharashtra (Fig. 3). The estimated size of the landslide area is 291,350.78 m^2 (29.13 ha) in the study region. The inventory mapping reveals that the west escarpment of the study region, extending from the central ridgeline, exhibits a steep slope and a high concentration of landslides. The majority of landslides on the inventory map are located on the western steep slope of the Ghat, while the upper plateau of the region shows a lower concentration of landslides. The steep slopes around Phondaghat, Kumbhavade, and Amboli exhibit a very high concentration of historical landslides. Based on their shape as recorded in the inventory, the majority of landslides in the study region are identified as debris flow and transitional landslides.

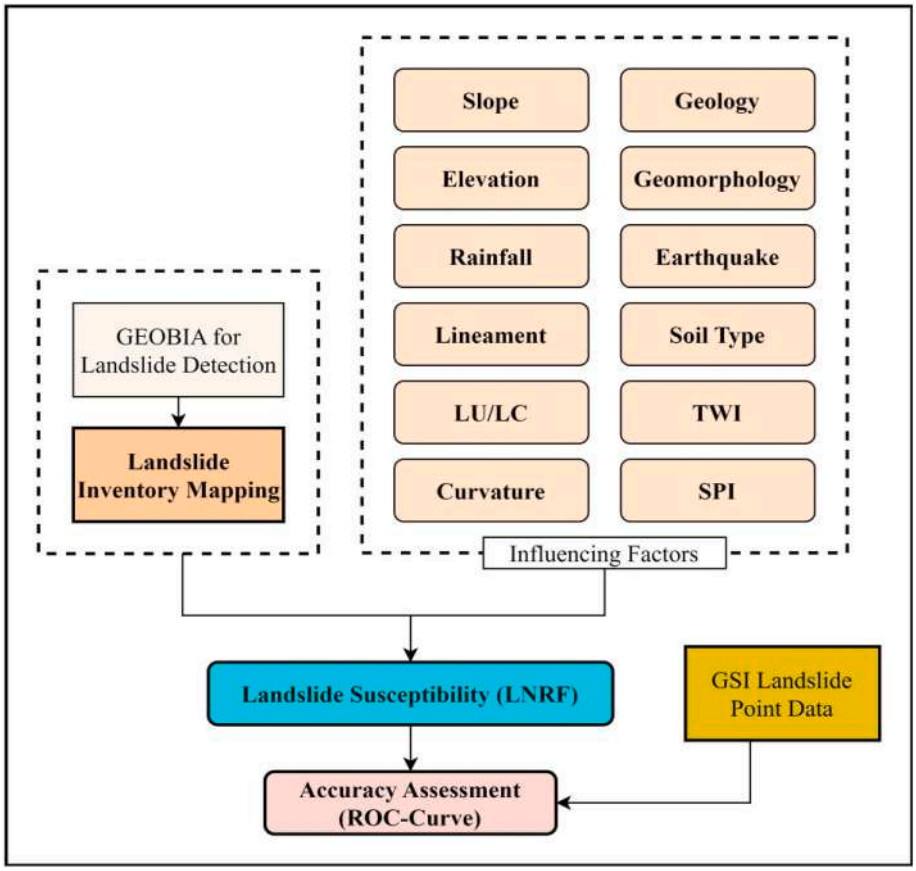

Fig. 2. Flowchart of research methodology.

3.2. Landslide influencing factors

3.2.1. Slope

The occurrence of landslides is significantly influenced by the gradient of the slope, which is a critical factor in landslide analysis that determines the severity and extent of the landslide. The stability of the slope is greatly affected by its geometry, and as the height of the slope increases, its stability decreases, resulting in more frequent and severe landslides on steep slopes compared to gentle slopes. Additionally, the slope determines the size and movement of the landslide, as supported by studies conducted by Donnarumma et al. (2013) and Chen et al. (2016). The slope of the study region is divided into seven categories (Fig. 4a): Gentle slope, Moderate slope, Strong slope, Very Strong slope, Extreme slope, Steep slope, and Very steep slope representing areas 24, 21, 29, 13, 9, 3, and 1 percent respectively. In the Extreme slope category, there are 39% of landslides, comprised of the largest number of

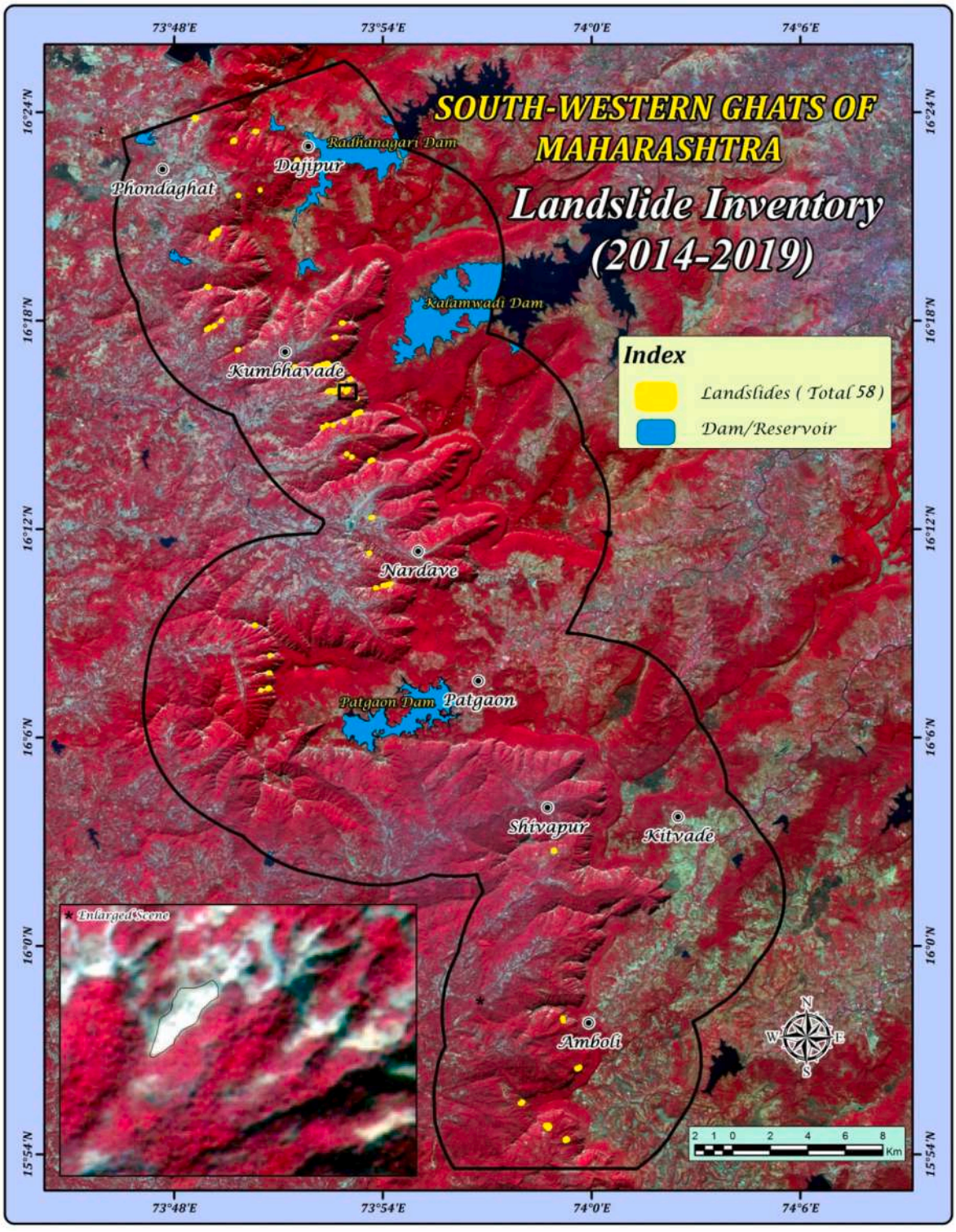

Fig. 3. Landslide inventory.

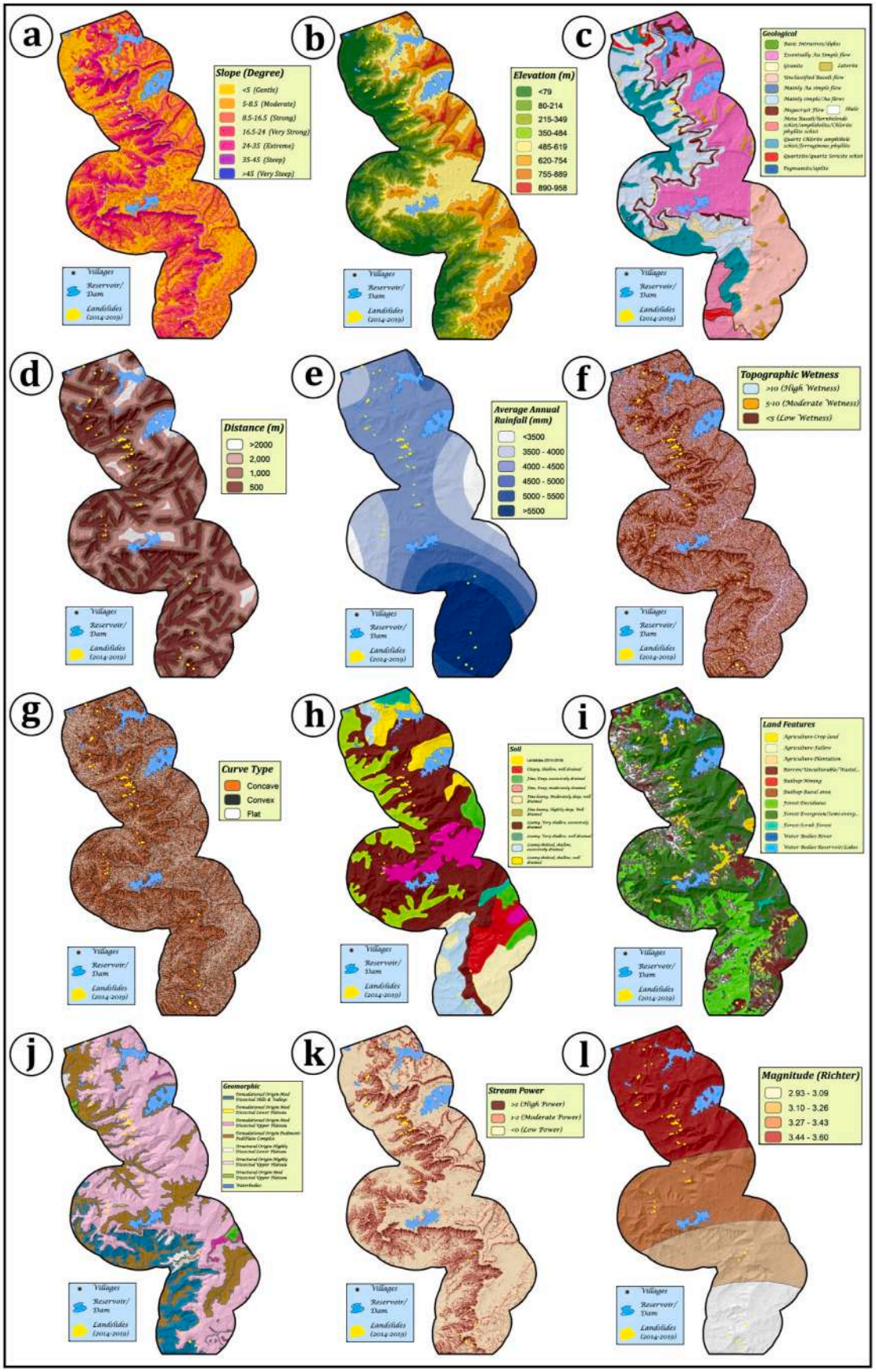

Fig. 4. Influencing factors (a) Slope; (b) Elevation; (c) Geology; (d) Lineament distance; (e) Rainfall; (f) TWI; (g) Topographic Curvature; (h) Soil; (i) LU/LC; (j) Geomorphology; (k) SPI; and (l) Earthquake.

landslides (Fig. 5a). However, the geographical allocation of landslides reduced as the gradient of the slope increased further. The removal of material at the bottom of a slope may increase the slope instability that triggers the landslide.

3.2.2. Elevation

According to Ercanoglu and Gokceoglu (2004), landslides are more likely to occur at higher altitudes. The Western Ghats region has a diverse topography with varying relief, comprising two major regions - Konkan and Ghati area. The elevation in both areas differs significantly, with the west section of the study region exhibiting the greatest elevation changes in the Konkan region, while the Ghati plateau region is relatively flat with the least elevation change. Deshpande (1971) notes that there are local variations in elevation variations that appeared in the west-east course of the Western Ghats. The study region shows the lowest height in the west part, with an elevation of only 5 m above the mean sea. The west part of the study region has the least height compared to the east part, which is characterized by higher elevations. The elevation is classified into eight classes in the study region viz. Less than 79 m (16%), 80–214 m (17%), 215–349 m (11%), 350–484 m (5%), 485–619 m (22%), 620–754 m (19%), 755–889 m (8%) and 890 to 958 (1%) (Fig. 4b). The maximum elevation is 958 m, which is detected along the ridge line of the Western Ghats in the study region. The highest concentration of landslides tends to be in the elevation range of 215–349 m (33% landslides) (Fig. 5b).

3.2.3. Geology

The stability of a slope and the type of weathering and erosion in a region are influenced by the composition of rocks (Citrabhuwana and Bahagiarti, 2016). The geology of a region determines the frequency and extent of landslides, with complex areas like the Himalayas and Deccan plateau posing threats such as earthquakes and landslides (Hubbard and Shaw, 2009). The Western Ghats indicates its uplift history, with a rugged and weak edge that has degraded from the Deccan Plateau. Therefore, it is crucial to consider the geology of the study region when assessing landslide susceptibility. The Geological Survey of India's map source is used to map the geology of the study region, as presented in Fig. 4c. The geographical allocation of geological formations in the

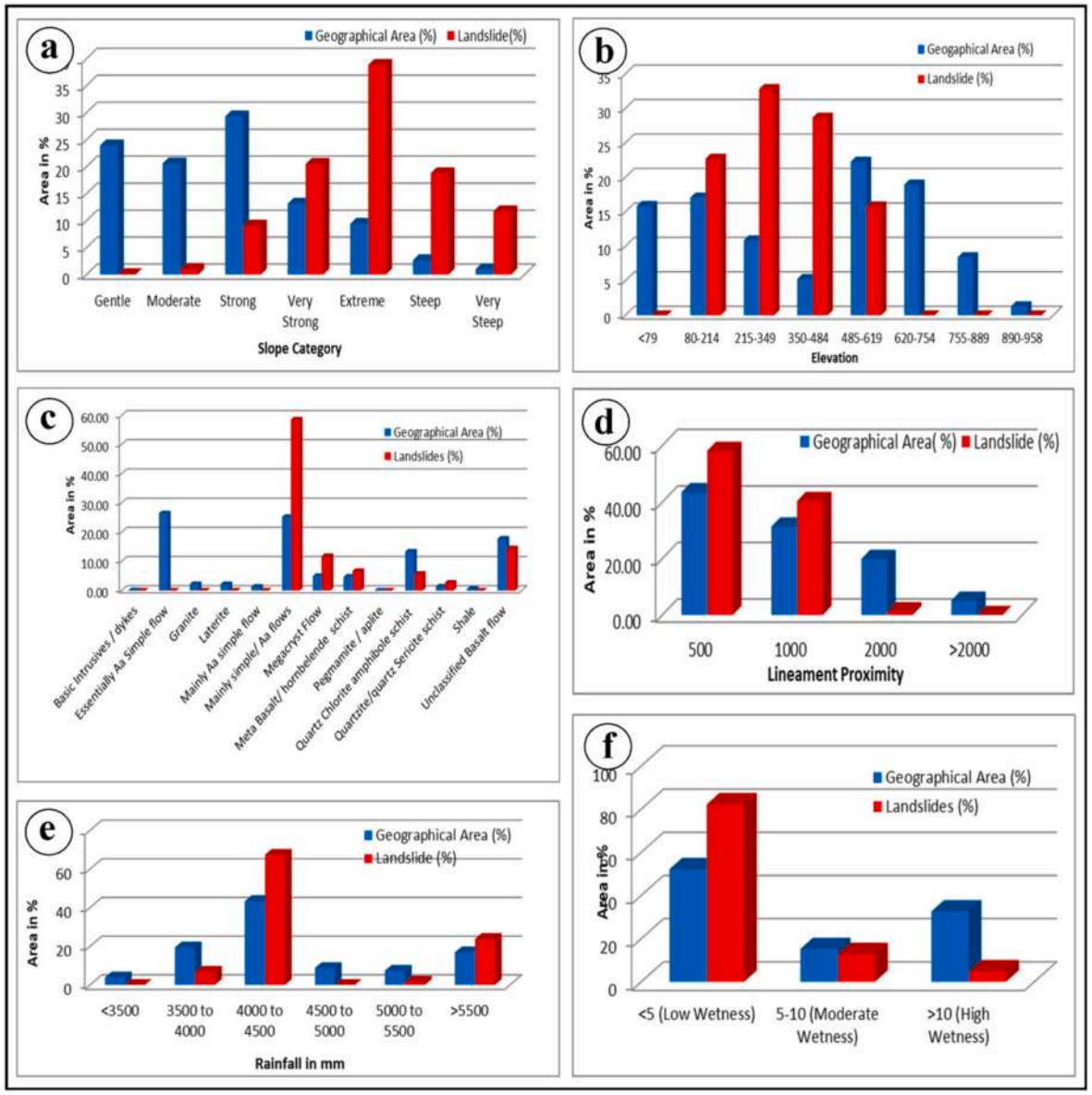

Fig. 5. (a) Slope vs. Landslide Inventory; (b) Elevation vs. Landslide Inventory; (c) Geology vs. Landslide Inventory; (d) Lineament distance vs. Landslide Inventory; (e) Rainfall vs. Landslide Inventory; and (f) TWI vs. Landslide Inventory.

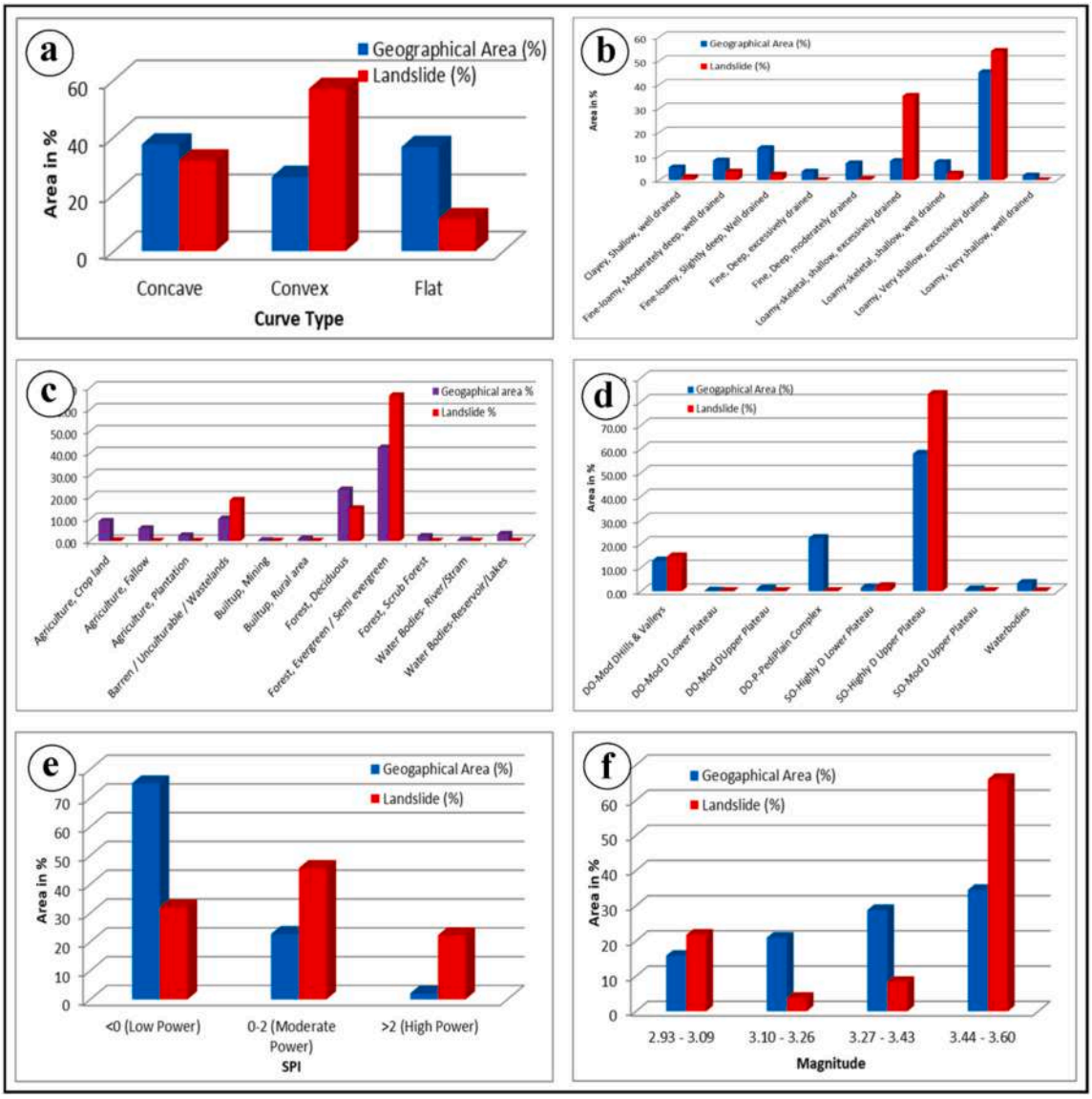

Fig. 6. (a) Topographic Curvature vs. Landslide Inventory; (b) Soil vs. Landslide Inventory; (c) LU/LC vs. Landslide Inventory; (d) Geomorphology vs. Landslide Inventory; (e) SPI vs. Landslide Inventory; and (f) Earthquake vs. Landslide Inventory.

study region is depicted on this map. The landslide inventory layer is then overlaid on the geological surface to illustrate the different types of rocks found in the study region. The maximum area is enclosed by rock formations of Essentially Aa Simple flow (26%), followed by Mainly simple/Aa flows (25%), Unclassified Basalt flow (18%), Quartz Chlorite amphibole schist/ferruginous phyllite (13%), Megacryst Flow (5%), Meta Basalt/hornblende schist (35), Laterite (2%), Granite (2%), Quartzite/quartz Sericite schist (1%), Mainly Aa simple flow (1%), Shale (1%), Basic Intrusives/dykes (<1%) Pegmamite/aplite (<1%). Landslides are seen to occur 60% of the incidence in the Mostly Aa simple flow rock category (Fig. 5c).

3.2.4. Lineament

Lineaments, which are linear features on the landscape that reveal underlying geological structures such as faults and joints, are important in understanding slope stability and landslide occurrences (Hobbs, 1904; Nagarajan et al., 1998). The degree of fracturing and joining with the slope, as well as the proximity to active fault zones, are critical factors in determining slope stability (Rodrigo et al., 2017). Landslides are more likely to occur in areas with linear patterns or lineaments (Nagarajan et al., 1998), and the existence of active faults can enhance the potential for landslides due to the weakening of rocks near the fault through extreme shearing (Leir et al., 2004).

The lineaments are identified and mapped in the study region by using remote sensed data (about the Bhuvan web portal of NRSC) and GIS techniques. The NRSC produced a lineament map at a scale of 1:50,000, with most lineaments being identified along stream valleys (Fig. 4d). Proximity zones are determined for the investigation by using a buffer around the lineament, as per the studies by Saha et al. (2005) and Ramli et al. (2010). The lineament distance of the study region is divided into four categories: 500 m, 1000 m, 2000 m, and >2000 m, representing 44%, 31%, 20%, and 5% area, respectively. There are 58%

Table 1
The unit weight based on the LNRF method (Ali Mohammadi et al., 2014b; Gupta and Joshi, 1990).

LNRF	Weight
<0.67	0
0.67–1.33	1
>1.33	2

landslides in the 500 m buffer zone, comprising the highest number of landslides (Fig. 5d).

3.2.5. Rainfall

Several studies (Chen and Lee, 2003; Edier et al., 2016; Ogbonnaya, 2015) have identified rainfall as a significant trigger for slope instability and landslides. In mountainous areas, landslides are often associated with either short-term rainstorms of high intensity or prolonged periods of low to moderate rainfall (Guzzetti et al., 2008).

The study region is characterized by extreme rainfall on the west mountain slope in the southwest monsoon season, whereas the east slope receive milder rainfall. This high variation in rainfall patterns throughout the Western Ghats results in a diverse range of vegetation categories. To obtain average annual rainfall data for the last 8 years, 71 surrounding stations of the Department of Agriculture, Government of Maharashtra are used, and the data is freely available on the official website https://maharain.maharashtra.gov.in/. Point data from the rainfall stations is interpolated using Kriging-Exponential interpolation techniques, and the average annual rainfall is found to range from 3039 mm to 6177 mm (Fig. 4e). The study region is classified into six categories based on the average annual rainfall: <3500 mm (4%), 3500–4000 mm (19%), 4000–4500 mm (43%), 4500–5000 mm (9%), 5000–5500 mm (7%) and >5500 mm (17%). Most of the landslide incidences are found in the 4000–4500 mm (67% landslides) rainfall range (Fig. 5e).

3.2.6. Topographic Wetness Index (TWI)

In 1979, Beven and Kirkby 1979 created the Topographic Wetness Index (TWI) as part of the runoff model known as TOPMODEL. This index can identify locations that accumulate precipitation, even in areas with seasonally or permanently saturated surfaces. Consequently, it is a valuable tool for characterizing the geomorphology of landslides, including the spatial arrangement of elevated regions that remain relatively dry and low-lying areas that tend to be wet. Rozycka et al. (2017) found this index to be particularly useful for describing landslide features.

In this research, TWI is generated from a digital elevation model (DEM) using the topographic wetness formula in ArcGIS 10.7.1. The resulting TWI is then classified into three categories: Low wetness (52%), Moderate wetness (15%), and High wetness (33%). The upper slope of the study region exhibited lower wetness, while the slope toe showed higher wetness due to the likelihood of water accumulation. The majority of landslides are found in areas classified as Low wetness (82% landslides), followed by Moderate wetness (13% landslides) and High wetness (5% landslides) as shown in Fig. 4f and Fig. 5f.

3.2.7. Topographic curvature

Topographic curvature is a crucial factor to consider in the analysis of landslide susceptibility. It provides information on the terrain condition of an area and its slope morphology, as well as the movement of water (Akinci et al., 2011). Mathematically, the curvature is the change in the angle of the slope over an extremely narrow curve's arc (Thomas, 1968), which is the inverse of the circumference of a circle that is tangential to the curve at a minimum of three times (Kepr, 1969).

For this research, digital elevation data is utilized to derive the plan curvature of the slope for landslide hazard evaluation. The plan curvature is categorized into three types: concave (positive curve), convex (negative curve), and flat (zero curve) (Qiqing et al., 2015), which cover approximately 52%, 57%, and 37% of the area, respectively (as shown in Fig. 4g). The Convex areas (57% landslide) tend to have the highest concentration of landslides (Fig. 6a).

3.2.8. Soil

To identify conditions of vulnerability to landslides, it is important to understand the hydrological processes that involve soil and relief. This knowledge is essential in the fields of environmental studies and risk reduction. Soil properties and relief forms significantly affect water infiltration and storage capacity in the soil, which, in turn, influence the likelihood of landslides (Petschko et al., 2014). Therefore, having information on these factors is crucial in assessing landslide susceptibility.

In this study, a soil map of the study region is created using data from the Geological Survey of India and the National Bureau of Soil Survey, India (as shown in Fig. 4h). The soil in the area is classified in to nine types. Among these, the majority of landslide incidents occurred in the Loamy, Very shallow, excessively drained soil type (54% landslides), followed by the Loamy-skeletal, shallow, excessively drained soil type (35% landslides) (Fig. 6b).

3.2.9. Land use/land cover (LU/LC)

The environmental and socio-economic aspects of the surface of the earth are represented by LU/LC (Mohammed et al., 2014). It is a critical element in understanding the relationship between human actions and the environment (Rajan and Shibasaki, 2001). In addition to various influencing factors affecting the spatial distribution of landslides, LU/LC dynamics are also an important factor in landslide mapping (Guillard and Zezere, 2012). Land use and land cover changes, such as deforestation, slope ruptures, and steep slopes, can accelerate slope instability (Reichenbach et al., 2014). Land management activities, often in association with natural conditions like flooding or earthquakes, can transform moderately stable hill slopes into landslides.

An integrated approach of object-oriented classification of LISS-4 image and reference use of the Google Earth software platform is used to produce the LU/LC map of the study region (Fig. 4i). The simplified map depicts LU/LC units such as Agriculture-Crop land (9%), Agriculture-Plantation (2%), Agriculture-Fallow (6%), Barren/Unculturable/Wastelands (10%), Builtup-Rural area and mining (1%), Forest-Deciduous (23%), Forest-Evergreen/Semi-evergreen (43%), Forest-Scrub Forest (2%), Wetlands/Water Bodies-Reservoir/River/Lakes (4%). The analysis indicates that a vast area of the study region (68%) is enclosed by forest, which is a very high percentage. As per the landslide inventory, most of the landslide incidences occurred in Forest-Evergreen/Semi-evergreen (66%), followed by Barren/Unculturable/Wastelands (19%) (Fig. 6c).

3.2.10. Geomorphology

Geomorphology is a scientific field that examines the inception, process, and development of landforms and their role in shaping landscape design (Stetler, 2014). The Southern Indian tectonic shield is thought to have been made through a gradual geomorphic procedure (Radhakrishna, 1993). To obtain information about the study region's geomorphology, data from the NGLM (National Geomorphology and Lineament Mapping) project's database, available on NRSC's Bhuvan website, is utilized (Fig. 4j).

In the study region, there are eight distinct geomorphic landforms. The highest concentration of landslides, at 83%, is found in the Structural Origin-Highly Dissected Upper Plateau. The Denudational Origin-Mod Dissected Hills & Valleys category comes second, with 15% of landslides. The remaining categories have a concentration of landslides of less than 3%. Fig. 6d illustrates the distribution of geomorphic units and the number of landslides present in each respective unit.

3.2.11. Stream power index (SPI)

SPI is a crucial factor in defining the stability of the study region, as it measures the erosive power of flowing water or streams, which is one of the leading contributing factors to stability (Moore and Grayson, 1991; Conforti et al., 2011; Regmi et al., 2014). It estimates the potential of streams to change the geomorphic features of the region by causing gully erosion and transport. The SPI method is useful in identifying areas where overland flow in the catchment has a greater capacity to erode the terrain (Wilson and Gallant, 2000). Therefore, incorporating the SPI method in erosion and terrain susceptibility modeling is significant.

To compute the SPI for the study region, the digital elevation model

Table 2
The results of integration of landslide layer with influencing factors (**LNRF**).

Influencing Factors			Area Units		Landslide Area		Analysis		
Factors	No. Of Classes	Class	Area (Ha.)	Geographical Area (%)	Area (Ha.)	Landslide Area (%)	LNRF (A/E)	Weight	Instability
Slope	1	<5° (Gentle Slope)	25,907	23.92	0.02	0.06	0.00	0	Low
	2	5°–8.5° (Moderate Slope)	22,287	20.58	0.30	1.02	0.07	0	Low
	3	8.5°–16.5° (Strong Slope)	31,735	29.31	2.65	9.08	0.64	0	Low
	4	16.5°–24° (Very Strong Slope)	14,232	13.14	5.97	20.50	1.44	2	High
	5	24°–35° (Extreme Slope)	10,196	9.42	11.32	38.84	2.72	2	High
	6	35°–45° (Steep Slope)	2868	2.65	5.47	18.78	1.31	1	Medium
	7	>45° (Very Steep Slope)	1060	0.98	3.41	11.72	0.82	1	Medium
Geology	1	Basic Intrusives/dykes	51	0.05	0.00	0	0.00	0	Low
	2	Essentially Aa Simple flow	28,606	26.42	0.00	0	0.00	0	Low
	3	Granite	2383	2.20	0.00	0	0.00	0	Low
	4	Laterite	2407	2.22	0.00	0	0.00	0	Low
	5	Mainly Aa simple flow	1382	1.28	0.00	0	0.00	0	Low
	6	Mainly simple/Aa flows	27,259	25.17	17.50	58.54	7.61	2	High
	7	Megacryst Flow	5377	4.97	3.54	11.84	1.54	2	High
	8	Meta Basalt/hornbelende schist …	5102	4.71	2.00	6.69	0.87	1	Medium
	9	Pegmamite/aplite	10	0.01	0.00	0.00	0.00	0	Low
	10	Quartz Chlorite amphibole schist …	14,452	13.35	1.73	5.79	0.75	1	Medium
	11	Quartzite/quartz Sericite schist	1445	1.33	0.80	2.68	0.35	0	Low
	12	Shale	573	0.53	0.00	0.00	0.00	0	Low
	13	Unclassified Basalt flow	19,238	17.77	4.32	14.45	1.88	2	High
Geomorphology	1	Denudational Origin-Mod Dissected Hills & Valleys	13,995	12.92	4.28	14.70	1.18	1	Medium
	2	Denudational Origin-Mod Dissected Lower Plateau	140	0.13	0.00	0.00	0	0	Low
	3	Denudational Origin-Mod Dissected Upper Plateau	1094	1.01	0.00	0.00	0	0	Low
	4	Denudational Origin-Pediment-PediPlain Complex	24,195	22.34	0.00	0.00	0	0	Low
	5	Structural Origin-Highly Dissected Lower Plateau	1686	1.56	0.61	2.10	0.17	0	Low
	6	Structural Origin-Highly Dissected Upper Plateau	62,732	57.93	24.24	83.20	6.66	2	High
	7	Structural Origin-Mod Dissected Upper Plateau	767	0.71	0.00	0.00	0.00	0	Low
	8	Waterbodies	3677	3.40	0.00	0.00	0.00	0	Low
Lineament	1	<500 m	47,147	43.54	16.95	58.18	2.33	2	High
	2	500–1000 m	33,956	31.36	11.79	40.46	1.62	2	High
	3	1000–2000 m	21,572	19.92	0.40	1.36	0.05	0	Low
	4	>2000 m	5610	5.18	0.00	0.00	0.00	0	Low
Elevation	1	<79 m	17,179	15.87	0.00	0.00	0.00	0	Low
	2	80–214 m	18,470	17.06	6.61	22.71	1.82	2	High
	3	215–349 m	11,767	10.87	9.56	32.82	2.63	2	High
	4	350–484 m	5691	5.26	8.35	28.67	2.29	2	High
	5	485–619 m	24,129	22.28	4.60	15.79	1.26	1	Medium
	6	620–754 m	20,512	18.94	0.00	0	0.00	0	Low
	7	755–889 m	9113	8.42	0.00	0	0.00	0	Low
	8	890–958 m	1425	1.32	0.00	0	0.00	0	Low
Earthquake	1	2.93–3.09	17,122	15.81	6.35	21.79	0.87	1	Medium
	2	3.10–3.26	22,663	20.93	1.12	3.83	0.15	0	Low
	3	3.27–3.43	31,149	28.77	2.45	8.39	0.34	0	Low
	4	3.44–3.60	37,351	34.49	19.23	65.99	2.64	2	High
LULC	1	Agriculture, Crop land	9765	9.02	0.05	0.17	0.02	0	Low
	2	Agriculture, Fallow	6120	5.65	0.00	0.00	0.00	0	Low
	3	Agriculture, Plantation	2638	2.44	0.00	0.00	0.00	0	Low
	4	Barren/Unculturable/Wastelands	10,932	10.10	5.43	18.64	2.05	2	High
	5	Builtup, Mining	255	0.24	0.00	0.00	0.00	0	Low
	6	Builtup, Rural area	996	0.92	0.00	0.00	0.00	0	Low
	7	Deciduous Forest	25,299	23.36	4.31	14.79	1.63	2	High
	8	Evergreen/Semi-evergreen	46,041	42.52	19.35	66.40	7.30	2	High
	9	Forest, Scrub Forest	2320	2.14	0.00	0	0.00	0	Low
	10	River/Stream	526	0.49	0.00	0	0.00	0	Low
	11	Reservoir/Lakes/Ponds	3393	3.13	0.00	0	0.00	0	Low
Rainfall	1	<3500 mm	4233	3.91	0.00	0	0.00	0	Low
	2	3500–4000 mm	21,084	19.47	2.02	6.94	0.42	0	Low
	3	4000–4500 mm	47,021	43.42	19.64	67.43	4.05	2	High
	4	4500–5000 mm	9582	8.85	0.00	0.00	0.00	0	Low
	5	5000–5500 mm	8037	7.42	0.51	1.73	0.10	0	Low
	6	>5500 mm	18,327	16.93	6.96	24	1.43	2	High
Topographic Curvature	1	Concave	40,548	37.45	9.26	31.79	0.95	1	Medium
	2	Convex	28,159	26.00	16.59	56.95	1.71	2	High
	3	Flat	39,578	36.55	3.28	11.26	0.34	0	Low

(*continued on next page*)

Table 2 (*continued*)

Influencing Factors			Area Units		Landslide Area		Analysis		
Factors	No. Of Classes	Class	Area (Ha.)	Geographical Area (%)	Area (Ha.)	Landslide Area (%)	LNRF (A/E)	Weight	Instability
Soil Type	1	Clayey, shallow, well-drained	5750	5.31	0.38	1.29	0.12	0	Low
	2	Fine-loamy, moderately deep, well-drained	8845	8.17	1.05	3.61	0.33	0	Low
	3	Fine-loamy, slightly deep, well drained	14,447	13.34	0.67	2.29	0.21	0	Low
	4	Fine, deep, excessively drained	3821	3.53	0.00	0.00	0.00	0	Low
	5	Fine, deep, moderately drained	7586	7.01	0.17	0.57	0.05	0	Low
	6	Loamy-skeletal, shallow, excessively drained	8655	7.99	10.29	35.32	3.18	2	High
	7	Loamy-skeletal, shallow, well drained	8113	7.49	0.81	2.77	0.25	0	Low
	8	Loamy, very shallow, excessively drained	49,007	45.26	15.78	54.15	4.87	2	High
	9	Loamy, very shallow, well drained	2062	1.90	0.00	0.00	0.00	0	Low
SPI	1	<0 (Low Power)	81,364	75.14	9.32	31.99	0.96	1	Medium
	2	0-2 (Moderate Power)	24,649	22.76	13.30	45.65	1.37	2	High
	3	>2 (High Power)	2273	2.10	6.52	22.36	0.67	1	Medium
TWI	1	<5 (Low Wetness)	56,489	52.17	23.95	82.21	2.47	2	High
	2	5-10 (Moderate Wetness)	16,499	15.24	3.76	12.91	0.39	0	Low
	3	>10 (High Wetness)	35,298	32.60	1.42	4.88	0.15	0	Low
	Total		**108,285**	**100**	**29.134**	**100**			

*LNRF=Landslide Numerical Risk Factor *A = Geographical Area of Class *E = Mean Area of Landslide.

is used as input data, and the SPI module available in SAGA software is utilized. The SPI values in the study region range from −3 to 5, representing the varying erosive power of the rivers in the area. Higher SPI values signify the potential for overland flow paths in heavy rainfall, which can result in gully erosion or other erosion-prone areas. In this study, the SPI values are classified into three categories: <0 (Low Power) (75%), 0–2 (Moderate Power) (23%), and >2 (High Power) (2%) (Fig. 4k). Most of the landslide incidences occurred in the Moderate Power category (46% Landslide), followed by the Low Power category (32% Landslide) and the High Power category (22% Landslides) (Fig. 6e).

3.2.12. Earthquake

The occurrence of landslides can be influenced by various factors, and earthquakes are one of the significant triggering causes (Wang et al., 2014). To analyze the hazard associated with earthquake-induced landslides, it is essential to consider both landslide and seismic hazards (Martino et al., 2019). In this study, earthquake data is analyzed by interpolating reported magnitudes at different locations. Earthquake magnitudes are reported by IMD and Earthquake bulletins. The earthquakes in the study region ranged from 2.93 to 3.6 on the Richter scale, which falls in the medium range of magnitudes. The interpolated earthquake map divides the study region into four zones based on magnitude: 2.93–3.09 (16%), 3.10–3.26 (21%), 3.27–3.43 (29%), and 3.44–3.60 (34%) (Fig. 4l). The highest concentration of landslides is found in the 3.44 to 3.60 magnitude earthquake category, with 66% of landslides occurring in this zone (Fig. 6f).

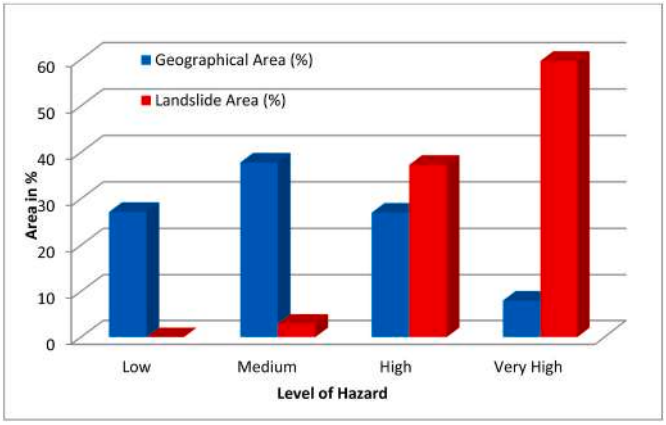

Fig. 7. Landside Hazard (LNRF) vs. Landslide Inventory.

3.3. Landslide Numerical Risk Factor (LNRF)

Gupta and Joshi (1990) proposed a model for zoning landslide susceptibility using GIS known as LNRF, which is a useful method, particularly for hilly regions. Moreover, a review of the literature revealed certain findings of research such as Gupta and Joshi (1990); Mohammed et al. (2014a), and Malik et al. (2016) suggested that the LNRF system has an effective approach for mapping landslide susceptibility mapping. The occurrence of the landslide includes multiple natural and human factors. Therefore, for this research work, influencing factors are selected, and weighted values are determined for each phenomenon using the LNRF model. In this analysis, the weight of every class is determined by dividing the number of landslides (Landslide Inventory, 2014–2019) in one unit by the mean of landslides in whole units. The weights of the LNRF are calculated using equation (1) for each influencing factor. The LNRF weights of each factor are attached to the corresponding attribute table of the influencing factor. All influencing factors are integrated with their respective tables for the attributes. This model is calculated from the following formula:

$$LNRF = A / E \text{ (Mohammadi et al., 2014a)} \quad (1)$$

Where.

A is the landslide area in each unit, and
E is the average area of the landslide in the all unit.

As per equation (1), the weight of every homogeneous unit is assessed and related tables are made for weighted maps. LNRF is determined for each homogeneous unit in three groups of low instability (0), medium (1), and high (2) as per (Table 1) At last, the zonation map of the landslide is prepared by integrating all derived weights of each influencing factor (Patil A. et al., 2020).

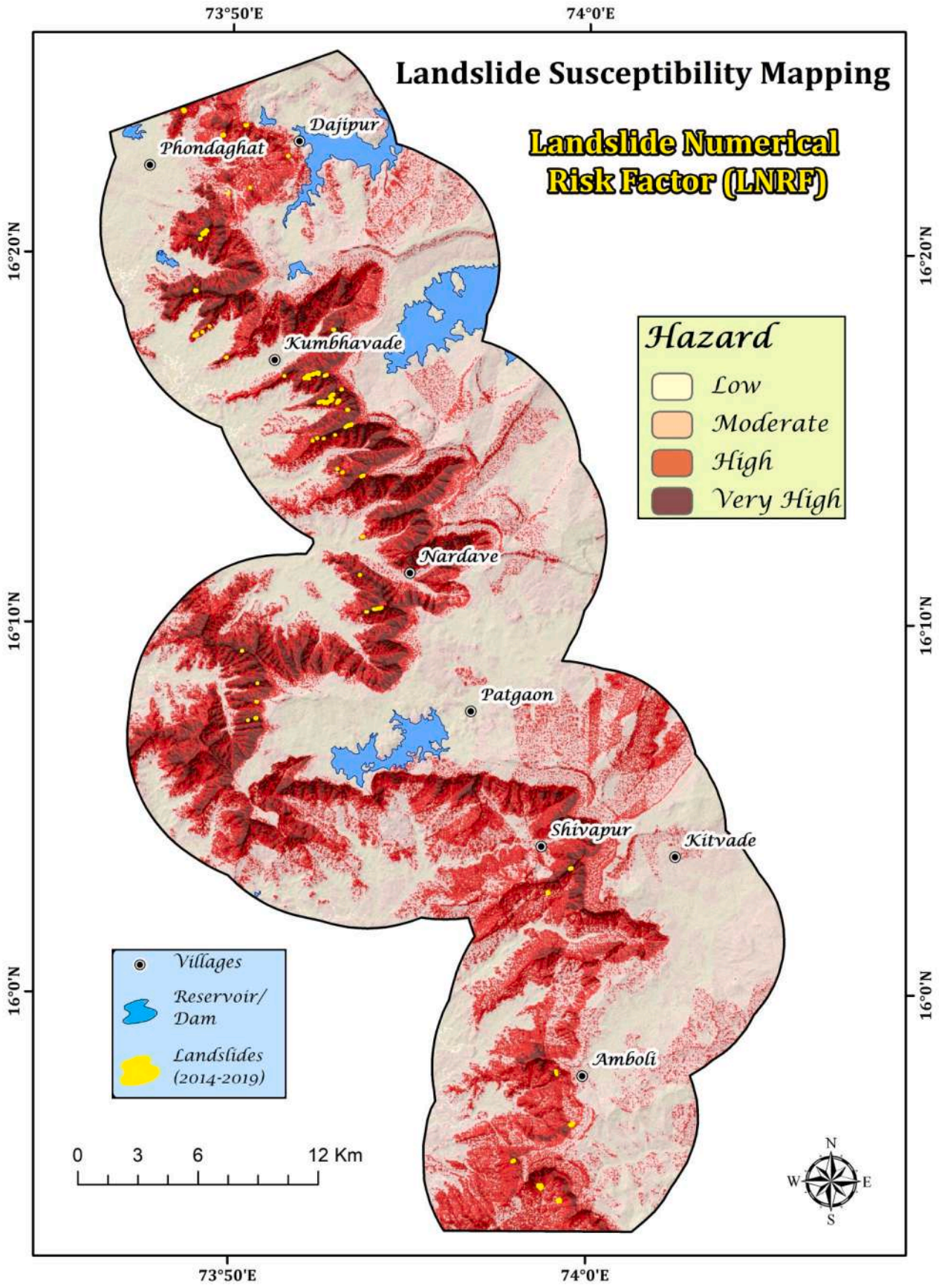

Fig. 8. Landslide hazard zonation using LNRF model.

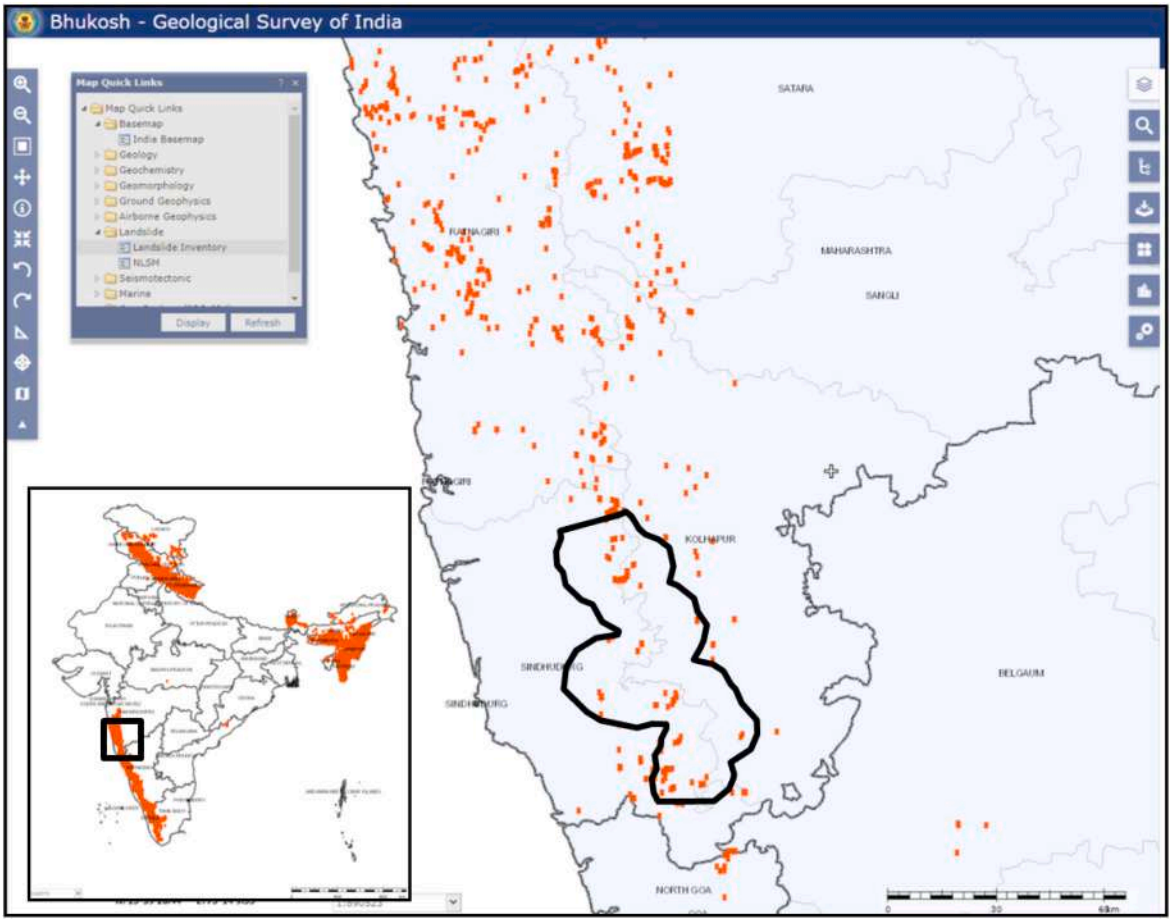

Fig. 9. Landslide point inventory by GSI.

4. Result and discussion

4.1. Landslide susceptibility map

The Landslide Number Rating Factor (LNRF) was calculated by integrating twelve influencing factors (Geology, Geomorphology, Slope, Elevation, Lineament, SPI, Earthquake, Rainfall, Soil, TWI, LU/LC, and Topographic curvature) with the landslide inventory layer. The tabular results of the LNRF model are shown in Table 2. LNRF values greater than 1 indicate that the influencing factors have a high responsibility for landslide occurrences, while values below 1 suggest that the factors are more consistent and have less influence on landslides (Gupta and Joshi, 1990).

For the slope factor, the class of 24°–35° (LNRF = 2.72) has the greatest influence on landslide occurrences in the study region. Steep hillsides prone to instability are caused by situations where the shear stress on the slope surpasses its resistance. Human activities such as road construction and changes in land use and land cover exacerbate this issue. On the other hand, flat areas (LNRF = 0) do not significantly affect landslide occurrences.

Regarding the geology parameter, the geologic units of mainly simple/Aa flows, unclassified basalt flow, and megacryst flow (LNRF = 7.61, 1.88, and 1.54, respectively) have a greater impact on landslide occurrences in the study region compared to other geologic units. These structures create favorable conditions for landslides as water infiltrates (Hong et al., 2016).

The analysis using the LNRF method reveals that elevation has a significant impact on landslide occurrences (Table 2). The class of 215–349 m shows a strong correlation with landslides, as indicated by its high LNRF value of 2.23. However, it should be noted that the occurrence of landslides initially increases with increasing elevation up to certain categories, after which it starts to decrease.

The LNRF method also highlights a significant correlation between topographic curvature classes and landslides. Both convex and concave surfaces show a stronger correlation with landslide occurrences, with LNRF values of 1.71 and 0.95, respectively. This is due to the divergence and convergence of water flow on these slopes, contributing to landslide occurrences (Hong et al., 2016; Chen et al., 2017).

The analysis of the Topographic Wetness Index (TWI) reveals that this factor has a significant impact on landslide occurrences. Interestingly, areas with the lowest wetness levels (less than 5) have the highest impact on landslide occurrences, indicated by the high LNRF value of 2.47. Conversely, areas with the highest wetness levels (between 5 and 10 and above 10) have the least influence, with LNRF values of 0.39 and 0.15, respectively.

The Specific Erosion Potential Index (SPI) results also highlight its major impact on landslide occurrences. Areas with moderate erosive stream power (between 0 and 2) have the highest impact, with an LNRF value of 1.37. Conversely, areas with the highest and lowest erosive stream power levels (less than 0 and greater than 2) have the least influence, with LNRF values of 0.96 and 0.67, respectively.

Linear factors such as lineaments also have significant effects on landslide occurrences. The classes of <500 m and 500–1000 m, representing the least distance from lineaments, have the highest LNRF values (2.33 and 1.62) and the most considerable effect on landslides. In contrast, the categories of 1000–2000 m and >2000 m, representing the highest distance from lineaments, have the lowest LNRF values (0.05 and 0.00). Geomorphology also plays a major role in landslide occurrences. The “Structural Origin-Highly Dissected Upper Plateau” category has the highest impact on landslide occurrences (LNRF = 6.66), while

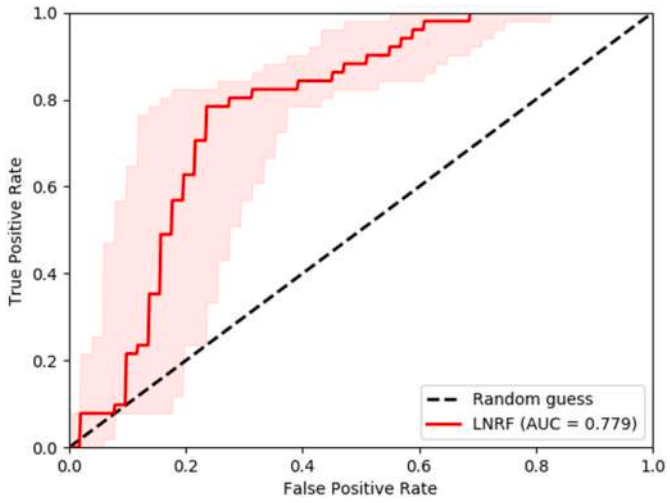

Fig. 10. ROC curve.

others have a relatively lower influence.

Based on the land use and land cover (LU/LC) categories, "Evergreen/Semi-evergreen forest," "Barren/uncultivated field," and "Deciduous forest" (LNRF = 7.30, 2.05, and 1.63, respectively) have the highest relation to landslide occurrences. Human activities, particularly deforestation, contribute to this correlation (Youssef et al., 2016). In terms of soil type, "Loamy, very shallow, excessively drained" and "Loamy-skeletal, shallow, excessively drained" (LNRF = 4.87 and 3.18, respectively) have a significant effect on landslides.

When combining rainfall and landslide maps in the LNRF model, it becomes apparent that areas with rainfall categories between 4000 and 4500 mm and greater than 5500 mm have a significant impact on landslide occurrences. These areas show a high LNRF value, indicating a strong correlation between high rainfall and landslide occurrences. Other rainfall categories have a relatively lower impact, suggesting their influence is less significant. The integration of earthquake and landslide maps in the LNRF model reveals that earthquake zones with magnitudes of 3.44–3.60 have a greater effect on landslide occurrences compared to other earthquake levels. All influencing variables are associated with landslides, leading to varying intensities of landslide occurrences.

The integrated result of the LNRF, as a landslide hazard index, ranges from 1 to 20. The highest value (20) reflects the sum of the largest weights of all 12 factors and indicates a high susceptibility region. The hazard index is categorized into four categories using the natural breaks (Jenks) method of classification: Low (27%), Moderate (38%), High (27%), and Very High (8%). It is notable that 60% of historical landslides are found in the Very High category, which covers only 8% of the land area. In contrast, no landslides have occurred in the low-hazard category (Fig. 7).

The areas around Dajipur, Nardave, and Amboli are considered dangerous for landslide incidence according to the LNRF results (Fig. 8). Phondaghat, Patgaon, and Kitavade villages fall under the categories of moderate and low landslide hazards. Areas further away from the foothills are much safer than those near the foot of the mountains. The high landslide hazard potential areas are found in the western part of the central mountain range, mostly categorized as a high and very high landslide susceptible zone.

4.2. Accuracy assessment

To assess the reliability and performance of the GIS-based LNRF technique in estimating areas susceptible to landslides, the receiver operating characteristic (ROC) method was employed. The ROC curve is a useful tool for evaluating the quality of a forecasting system, and the area under the curve (AUC) can be used to determine the overall model performance, where a higher AUC indicates better performance. In this study, the Geological Survey of India's landslide point inventory data was used as the testing data for the ROC method, as shown in Fig. 9.

The ROC curve was utilized to evaluate the overall performance of the landslide models on the 51 testing datasets. The success rate was determined by comparing the testing data with the landslide susceptibility map, as illustrated in Fig. 10. The LNRF model achieved an AUC value of 0.77, indicating good prediction performance and reliable results for the landslide susceptibility map. These findings suggest that the GIS-based LNRF technique is a reliable and effective method for estimating areas susceptible to landslides.

5. Conclusion

In conclusion, this study addresses the lack of research on landslide vulnerability in the Western Ghats of Maharashtra. By utilizing the LNRF model for landslide susceptibility mapping and integrating 12 influencing factors, the study provides valuable insights into the susceptibility of the region to landslides. The geology, land use/land cover, and geomorphology factors were found to have the most significant influence on the model.

The performance of the model was assessed using the ROC technique, which indicated good prediction performance. The susceptibility results showed that approximately 35% of the study region falls under high and very high landslide-susceptible zones. It is noteworthy that a significant number of historical landslides occurred in these high susceptibility zones.

Specific areas such as Dajipur, Shivapur, Nardave, and Amboli were identified as particularly dangerous for landslide incidents. On the other hand, Phondaghat, Patgaon, and Kitavade villages were found to have relatively lower susceptibility. Regions farther away from the foothills were also considered safer. The western region of the central mountain range, including Phonda Ghat and Amboli Ghat roads, was identified as having high potential landslide susceptibility.

The landslide susceptibility map generated through the LNRF model can serve as a valuable resource for planners and engineers. It can aid in identifying areas where preventive measures should be implemented to reduce the potential for future landslides. By utilizing this information, the impact of natural disasters can be minimized, contributing to the safety and well-being of local communities.

Overall, this research enhances our understanding of landslide susceptibility in the Western Ghats of Maharashtra and emphasizes the importance of proactive measures to mitigate the risks associated with landslides. The findings of this study can inform decision-making processes and help in the development of effective strategies to promote the resilience and safety of the region.

Declaration of competing interest

The authors declare that they have no known competing financial interests or personal relationships that could have appeared to influence the work reported in this paper.

Data availability

Data will be made available on request.

References

Abdo, H.G., 2022. Assessment of landslide susceptibility zonation using frequency ratio and statistical index: a case study of al-fawar basin, Tartous, Syria. Int. J. Environ. Sci. Technol. 19 (4), 2599–2618. https://doi.org/10.1007/s13762-021-03322-1.

Achour, Y., Pourghasemi, H.R., 2020. How do machine learning techniques help in increasing accuracy of landslide susceptibility maps? Geosci. Front. 11 (3), 871–883, 10.1016j.gsf.2019.10.001.

Ajin, R.S., Nandakumar, D., Rajaneesh, A., Oommen, T., Ali, Y.P., Sajinkumar, K.S., 2022. The tale of three landslides in the Western Ghats, India: lessons to be learnt. Influencing Disasters 9 (1). https://doi.org/10.1186/s40677-022-00218-1.

Akinci, H., Dogan, S., Kilicoglu, C., 2011. Production of landslide susceptibility map of Samsun (Turkey) City Center by using frequency ratio method. Int. J. Phys. Sci. 6 (5), 1015–1025.

Ali Mohammadi, Torkashvand, Akram, Irani, Jaliledin, Sorur, 2014b. The preparation of landslide map by landslide numerical risk factor (LNRF) model and geographic information system (GIS). The Egyptian Journal of Remote Sensing and Space Science 17 (2), 159–170. https://doi.org/10.1016/j.ejrs.2014.08.001. ISSN 1110-9823.

Beven, K.J., Kirkby, M.J., 1979. A physically based, variable contributing area model of basin hydrology. Hydrol. Sci. Bull. 24, 43–69.

Bhandari, R.K., Rawat, V., Bisht, S., Sati, S.K., 2020. Spatial analysis of landslide vulnerability using remote sensing and GIS techniques: a case study of Pithoragarh district, Uttarakhand, India. Geocarto Int. 35 (10), 1023–1042. https://doi.org/10.1080/10106049.2018.1484016.

Blaschke, T., Hay, G.J., Kelly, M., Lang, S., Hofmann, P., Addink, E., Feitosa, R.Q., van der Meer, F., van der Werff, H., van Coillie, F., Tiede, D., 2014. Geographic object-based image analysis - towards a new paradigm. ISPRS J. Photogrammetry Remote Sens. 87, 180–191. https://doi.org/10.1016/j.isprsjprs.2013.09.014.

Chen, H., Lee, C.F., 2003. A dynamic model for rainfall-induced landslides on natural slopes. Geomorphology 51 (4), 269–288.

Chen, X.L., Liu, C.G., Chang, Z.F., Zhou, Q., 2016. The relationship between the slope angle and the landslide size derived from limit equilibrium simulations. Geomorphology 253, 547–550. https://doi.org/10.1016/j.geomorph.2015.01.036.

Chen, W., Pourghasemi, H.R., Naghibi, S.A., 2017. A comparative study of landslide susceptibility maps produced using support vector machine with different kernel functions and entropy data mining models in China. Bull. Eng. Geol. Environ. 77, 1–18.

Citrabhuwana, K.B., Bahagiarti, K.P., 2016. Geology and slope stability analysis using markland method on road segment of piyungan – patuk, sleman and gunungkidul regencies, yogyakarta special region Indonesia. Int. j. econ. environ. Geol. 7 (1), 42–52.

Coco, L., Macrini, D., Piacentini, T., Buccolini, M., 2021. Landslide susceptibility mapping by comparing GIS-based bivariate methods: a focus on the geomorphological implication of the statistical results. Rem. Sens. 13 (21), 4280. https://doi.org/10.3390/rs13214280.

Conforti, M., Aucelli, P.P., Robustelli, G., Scarciglia, F., 2011. Geomorphology and GIS analysis for mapping gully erosion susceptibility in the Turbolo stream catchment (northern Calabria, Italy). Nat. Hazards 56 (3), 881–898.

Constantin, M., Bednarik, M., Jurchescu, M.C., Vlaicu, M., 2011. Landslide susceptibility assessment using the bivariate statistical analysis and the index of entropy in the Sibiciu Basin (Romania). Environ. Earth Sci. 63 (2), 397–406.

Dai, F.C., Lee, C.F., Li, J., Xu, Z.W., 2001. Assessment of landslide susceptibility on the natural terrain of Lantau Island, Hong Kong. Environ. Geol. 40 (3), 381, 39.

Daniel, H., Barbara, F., Clemens, E., 2015. An object-based approach for semi-automated landslide change detection and attribution of changes to landslide classes in northern Taiwan. Earth Sci Inform 8, 327–335.

Deshpande, C.D., 1971. Geography of Maharashtra, vol. 16. National book trust, India A-5 Green Park, New Delhi.

Devkota, K.C., Regmi, A.D., Pourghasemi, H.R., Yoshida, K., Pradhan B Ryu, I.C., et al., 2013. Landslide susceptibility mapping using certainty factor, index of entropy and logistic regression models in GIS and their comparison at Mugling–Narayanghat road section in Nepal Himalaya. Nat. Hazards 65 (1), 135–165.

Donnarumma, A., Revellino, P., Grelle, G., Guadagno, F.M., 2013. Slope angle as indicator parameter of landslide susceptibility in a geologically complex area. Landslide Science and Practice 425–433. https://doi.org/10.1007/978-3-642-31325-7-56.

Edier, Aristizábal, Jaime, I.V., Hernán, E.M., Michel, J., 2016. SHIA_Landslide: a distributed conceptual and physically based model to forecast the temporal and spatial occurrence of shallow landslides triggered by rainfall in tropical and mountainous basins. Landslides 13 (3), 497.

Ercanoglu, M., Gokceoglu, C., 2004. Use of fuzzy relations to produce landslide susceptibility map of a landslide prone area (West Black Sea Region, Turkey). Eng. Geol. 75, 229.

Froude, M.J., Petley, D.N., 2018. Global fatal landslide occurrence from 2004 to 2016. Nat. Hazards Earth Syst. Sci. 18 (8), 2161–2181. https://doi.org/10.5194/nhess-18-2161-2018.

Guillard, C., Zezere, J., 2012. Landslide susceptibility assessment and validation in the framework of municipal planning in Portugal: the case of loures municipality. Environ. Manag. 50, 721–735. https://doi.org/10.1007/s00267-012-9921-7.

Gupta, R.P., Joshi, B.C., 1990. Landslide hazard zoning using the GIS-approach, a case study from the Ramanga Catchment Himalayas. Eng. Geol. 28, 119–131.

Guzzetti, F., Carrara, A., Cardinali, M., Reichenbach, P., 1999. Landslide hazard evaluation: a review of current techniques and their application in a multi-scale study, Central Italy. Geomorphology 31, 181–216.

Guzzetti, F., Galli, M., Reichenbach, P., Ardizzone, F., Cardinali, M., 2006. Landslide hazard assessment in the collazzone area, Umbria, central Italy. Nat. Hazards Earth Syst. Sci. 6 (1), 115–131. https://doi.org/10.5194/nhess-6-115-2006.

Guzzetti, F., Peruccacci, S., Rossi, M., Stark, C.P., 2008. The rainfall intensity–duration control of shallow landslides and debris flows: an update. Landslides 5, 3–17.

Hadji, R., Rais, K., Gadri, L., Chouabi, A., Hamed, Y., 2017. Slope failure characteristics and slope movement susceptibility assessment using GIS in a medium scale: a case study from Ouled Driss and Machroha municipalities, Northeast Algeria. Arabian J. Sci. Eng. 42, 281–300.

Hobbs, W.H., 1904. Lineaments of the Atlantic border region. Geol. Soc. Am. Bull. 15, 483–506.

Hodasova, K., Bednarik, M., 2021. Effect of using various weighting methods in a process of landslide susceptibility assessment. Nat. Hazards 105, 481–499. https://doi.org/10.1007/s11069-020-04320-1.

Hong, H., Pradhan, B., Xu, C., Tien Bui, D., 2015. Spatial prediction of landslide hazard at the Yihuang Area (China) using two-class kernel logistic regression, alternating decision tree and support vector machines. Catena 133, 266–281. https://doi.org/10.1016/j.catena.2015.05.019.

Hong, H., Pourghasemi, H.R., Pourtaghi, Z.S., 2016. Landslide susceptibility assessment in Lianhua County (China): a comparison between a random forest data mining technique and bivariate and multivariate statistical models. Geomorphology 259, 105–118.

Hubbard, J., Shaw, J.H., 2009. Uplift of the longmen Shan and Tibetan plateau, and the 2008 wenchuan (M=7.9) earthquake. Nature 458, 194–197.

Hungr, O., Fell, R., Couture, R., Eberhardt, E. (Eds.), 2005. Landslide Risk Management, first ed. CRC Press. https://doi.org/10.1201/9781439833711.

Inamdar, N., 2021. Taliye Landslide: Locals Recall the Horror of Hillock Crashing onto Village, Burying 84. Hidusthan Times.

Iverson, R.M., 2018. Landslide triggering by rain infiltration. Water Resour. Res. 54 (9), 7269–7275. https://doi.org/10.1029/2018WR023243.

Kepr, B., 1969. Differential geometry. In: Rektorys, K. (Ed.), Survey of Applicable Mathematics. M.I.T. Press, Cambridge, pp. 298–372.

Lee, S., 2005. Application of logistic regression model and its validation for landslide susceptibility mapping using GIS and remote sensing data. Int. J. Rem. Sens. 26 (7), 1477–1491.

Lee, S., 2019. Current and future status of GIS-based landslide susceptibility mapping: a literature review. Korean J Remote Sens 35 (1), 179–193. https://doi.org/10.7780/KJRS.2019.35.1.12.

Leir, M., Michell, A., Ramsay, S., 2004. Regional landslide hazard susceptibility mapping for pipelines in British Columbia. In: Geo-engineering for the Society and its Environment. 57th Canadian Geotechnical Conference and the 5th Joint CGS-IAH Conference, October 24–27, Old Quebec, Canada, pp. 1–9.

Malik, R., Ghosh, S., Dhar, S., Singh, P., Singh, M., 2016. GIS based Landslide hazard from zonation along national highway AY-58, from Rishikesh to Joshimath, Uttarkhand, India. Int J Adv Remote Sens GIS Geogr 4 (2), 41–55.

Martha, T.R., Kerle, N., van Westen, C.J., Jetten, V., Kumar, K.V., 2012. Object oriented analysis of multi-temporal panchromatic images for creation of historical landslide inventories. ISPRS J. Photogrammetry Remote Sens. 67, 105–119. https://doi.org/10.1016/j.isprsjprs.2011.11.004.

Martino, S., Battaglia, S., D'Alessandro, F., Della Seta, M., Esposito, C., Martini, G., Troiani, F., 2019. Earthquake-induced landslide scenarios for seismic microzonation: application to the Accumoli area (Rieti, Italy). Bull. Earthq. Eng. https://doi.org/10.1007/s10518-019-00589-1.

Mohammed, N.B., Idowu, I.A., Benedine, A., 2014a. Analysis of land use-land cover changes in zuru and its environment of kebbi state, Nigeria using remote sensing and geographic information system technology. J. Geogr. Earth Sci. 2, 113–126.

Moore, I.D., Grayson, R.B., 1991. Terrain-based catchment partitioning and runoff prediction using vector elevation data. Water Resour. Res. 27 (6), 1171–1191.

Nagarajan, R., Mukherjee, A., Roy, A., Khire, M.V., 1998. Temporal remote sensing data and GIS application in landslide hazard zonation of part of Western Ghat, India. Int. J. Rem. Sens. 19, 573–585.

Ogbonnaya, Igwe, 2015. The study of the factors controlling rainfall-induced landslides at a failure-prone catchment area in Enugu, Southeastern Nigeria using remote sensing data. Landslides 12 (5), 1023.

Patil, A.S., Panhalkar, S.S., 2019. Analytical hierarchy process for landslide hazard zonation of South-Western ghats of Maharashtra, India. Disaster Adv 12 (5), 26–33.

Patil, A.S., Bhadra, B.K., Panhalkar, S.S., Patil, P.T., 2020. Landslide susceptibility mapping using landslide numerical risk factor model and landslide inventory prepared through OBIA in chenab valley, Jammu and Kashmir (India). J Indian Soc Remote Sens 48, 431–449. https://doi.org/10.1007/s12524-019-01092-5.

Patil, A.S., Panhalkar, S.S., Shinde, S.D., 2022. Frequency ratio approach for landslide susceptibility mapping of Phonda Ghat of Maharashtra. In: Singh, R.B., Kumar, M., Tripathi, D.K. (Eds.), Remote Sensing and Geographic Information Systems for Policy Decision Support. Advances in Geographical and Environmental Sciences. Springer, Singapore. https://doi.org/10.1007/978-981-16-7731-1_2.

Persichillo, M.G., Bordoni, M., Meisina, C., Bartelletti, C., Barsanti, M., Giannecchini, R., D'Amato Avanzi, G., Galanti, Y., Cevasco, A., Brandolini, P., Galve, J.P., 2016. Shallow landslides susceptibility assessment in different environments. Geomatics, Nat. Hazards Risk 8 (2), 748–771. https://doi.org/10.1080/19475705.2016.1265011.

Petschko, H., Brening, A., Bell, R., Goetz, J., Glade, T., 2014. Assessing the quality of landslide susceptibility maps – case study Lower Austria. Nat. Hazards Earth Syst. Sci. 14 (1), 95–118.

Pradhan, B., Lee, S., 2010. Landslide susceptibility assessment and Factor Effect Analysis: backpropagation artificial neural networks and their comparison with Frequency Ratio and bivariate logistic regression modelling. Environ. Model. Software 25 (6), 747–759. https://doi.org/10.1016/j.envsoft.2009.10.016.

Pradhan, B., Sezer, E.A., Gokceoglu, C., Buchroithner, M.F., 2010. Landslide susceptibility mapping by neuro-fuzzy approach in a landslide prone area (Cameron Highlands, Malaysia). Geoscience Remote Sensing, IEEE Trans 48 (12), 4164–4177.

Pradhan, B., Al-Najjar, H.A., Sameen, M.I., Mezaal, M.R., Alamri, A.M., 2020. Landslide detection using a saliency feature enhancement technique from LiDAR-derived DEM and orthophotos. IEEE Access 8, 121942–121954.

Pradhan, B., Sameen, M.I., Al-Najjar, H.A.H., Sheng, D., Alamri, A., Park, H.J., 2021. A meta-learning approach of optimisation for spatial prediction of landslides. Rem. Sens. 13 (22), 4521. https://doi.org/10.3390/rs13224521.

Qiqing, W., Wenping, L., Wei, C., Hanying, B., 2015. GIS-based assessment of landslide susceptibility using certainty factor and index of entropy models for the Qianyang County of Baoji city, China. J. Earth Syst. Sci. 124 (7), 1399–1415.
Radhakrishna, B.P., 1993. Neogene uplift and geomorphic rejuvenation of the Indian Peninsula. Curr. Sci. 64 (11&12), 787–793.
Raj, S.J., Chandrasekar, N., 2016. Landslide susceptibility mapping using frequency ratio model along eastern and western ghats of Tamil Nadu, India. J. Geol. Soc. India 87 (4), 423–433. https://doi.org/10.1007/s12594-016-0495-6.
Rajan, K., Shibasaki, R., 2001. A GIS based integrated land use/cover change model to study agricultural and urban land use changes. In: 22nd Asian Conference on Remote Sensing. Retrived from. https://crisp.nus.edu.sg/~acrs2001/pdf/250Rajan.pdf.
Ramachandra, T.V., Kumar, U., Bharath, H.A., Diwakar, P.G., Joshi, N.V., 2010. Landslide susceptible locations in western ghats: prediction through OpenModeller. In: Proceedings of the 26th Annual Symposium on Space and Technology ISROIISc Technology Cell. Indian Institute of Science, Bangalore.
Ramli, M.F., Yusof, N., Yusoff, M.K., Juahir, H., Shafri, H.Z.M., 2010. Lineament mapping and its application in landslide hazard assessment: a review. Bull. Eng. Geol. Environ. 69, 215–233. https://doi.org/10.1007/s10064-009-0255-5.
Regmi, A.D., Devkota, K.C., Yoshida, K., Pradhan, B., Pourghasemi, H.R., Kumamoto, T., Akgun, A., 2014. Application of frequency ratio, statistical index, and weights-of-evidence models and their comparison in landslide susceptibility mapping in Central Nepal Himalaya. Arabian J. Geosci. 7 (2), 725–742.
Reichenbach, P., Busca, C., Mondini, A.C., Rossi, M., 2014. The influence of land use change on landslide susceptibility zonation: the Briga catchment test site (Messina, Italy). Environ. Manag. 54, 1372–1384. https://doi.org/10.1007/s00267-014-0357-0.
Roccati, A., Paliaga, G., Luino, F., Faccini, F., Turconi, L., 2021. GIS-based landslide susceptibility mapping for land use planning and risk assessment. Land 10 (2), 162. https://doi.org/10.3390/land10020162.
Rodrigo, et al., 2017. Landslides Zonation Hazard: relation between geological structures and landslides occurrence in hilly tropical regions of Brazil. An. Acad. Bras. Cienc. 89 (4), 2609–2623.
Rozycka, M., Migon, P., Michniewicz, A., 2017. Topographic wetness index and terrain ruggedness index in geomorphic characterisation of landslide terrains, on examples from the sudetes, SW Poland. Z. Geomorphol. 61 (2), 61–80. https://doi.org/10.1127/zfg_suppl/2016/0328.
Saha, A.K., Gupta, R.P., Sarkar, I., Arora, M.K., Csaplovics, E., 2005. An approach for GIS-based statistical landslide susceptibility zonation—with a case study in the Himalayas. Landslides 2, 61–69.
Sarun, S., Vineetha, P., Reghunath, R., Sheela, A.M., Anil Kumar, R., 2021. Post landslide investigation of shallow landslide: a case study from the southern Western Ghats, India. Disaster Advances 14 (7), 52–59. https://doi.org/10.25303/147da5221.
Shano, L., Raghuvanshi, T.K., Meten, M., 2020. Landslide susceptibility evaluation and hazard zonation techniques – a review. Geoenviron Disasters 7 (18). https://doi.org/10.1186/s40677-020-00152-0.
Sidle, R.C., Tsuboyama, Y., Noguchi, S., Hosoda, I., Fujieda, M., Shimizu, T., Lusch, D.P., 2018. Landslides—processes, prediction, and land use. Water 10 (3), 307. https://doi.org/10.3390/w10030307.
Srivastava, V., Srivastava, H.B., Lakhera, R.C., 2010. Fuzzy gamma based geomatic modelling for landslide hazard susceptibility in a part of tons river valley, northwest Himalaya, India. Geomatics, Nat. Hazards Risk 1 (3), 225–242.
Stetler, L.D., 2014. In: Reference Module in Earth Systems and Environmental Sciences. Elsevier. https://doi.org/10.1016/B978-0-12-409548-9.05955-8.
Thomas, G.B., 1968. Calculus and Analytic Geometry: Part Two Vectors and Functions of Several Variables. Addison-Wesley Publishing, Reading, MA, USA, p. 784.
Vallabh, O., 2021. Taliye Landslide: Scores Join as Mass Ritual for 84 Victims Held at Mishap Site. The Indian Express.
van Westen, C.J., van Asch, T.W.J., Soeters, R., 2006. Landslide hazard and risk zonation—why is it still so difficult? Bull. Eng. Geol. Environ. 65 (2), 167–184. https://doi.org/10.1007/s10064-005-0023-0.
Vasudevan, N., Ramanathan, K., Parvathy, R.S., Ramesh, A., Joshy, K.V., 2022. Landscape degradation: the august 2019 puthumala landslide in Kerala, India. Lecture Notes in Civil Engineering 1–11. https://doi.org/10.1007/978-981-19-5077-3_1.
Wang, Ming, Liu, Min, Yang, Saini, Shi, Peijun, 2014. Incorporating triggering and environmental factors in the analysis of earthquake-induced landslide hazards. Int J Disaster Risk Sci 5, 125–135. https://doi.org/10.1007/s13753-014-0020-7.
Wang, Q., Li, W., Yan, S., Wu, Y., Pei, Y., 2016. GIS based frequency ratio and index of entropy models to landslide susceptibility mapping (Daguan, China). Environ. Earth Sci. 75 (9), 1–16.
Wilson, J.P., Gallant, J.C., 2000. Digital terrain analysis. Terrain Analysis: Principles and Applications 6 (12), 1–27.
World Health Organization, 2022. Landslides. https://www.who.int/news-room/fact-sheets/detail/landslides.
Youssef, A.M., Pourghasemi, H.R., Pourtaghi, Z.S., et al., 2016. Landslide susceptibility mapping using random forest, boosted regression tree, classification and regression tree, and general linear models and comparison of their performance at Wadi Tayyah Basin, Asir Region, Saudi Arabia. Landslides 13 (5), 839–856. https://doi.org/10.1007/s10346-015-0614-1.